inventions

MDPI

Article

Mathematical Modelling of Conveyor-Belt Dryers with Tangential Flow for Food Drying up to Final Moisture Content below the Critical Value

Dario Friso

Department of Land, Environment, Agriculture and Forestry, University of Padova, Agripolis, Viale dell'Università 16, 35020 Legnaro, Italy; dario.friso@unipd.it

Abstract: This work presents the mathematical modeling of the conveyor-belt dryer with tangential flow operating in co-current, which has the advantage of improving the preservation of the organoleptic and nutritional qualities of the dried food. On the one hand, it is a more cumbersome dryer than the perforated cross flow belt dryer but, on the other hand, it has a low air temperature in the final section where the product has a low moisture content and, therefore, it is more heat sensitive. The results of the mathematical modeling allowed a series of guidelines to be developed for a rational design of the conveyor-belt dryer with tangential flow for the specific case of the moisture content of the final product X_F lower than the critical one X_C ($X_F < X_C$). In fact, this work follows a precedent in which a mathematical model was developed through the differentiation of the drying rate equation along the dryer belt with the hypothesis that the final moisture content X_F of the product was higher than the critical one X_C. The relationships between the extensive quantities (air flow rate and product flow rate), the intensive quantities (temperatures, moisture content and enthalpies) and the dimensional ones (length and width of the belt) were then obtained. Finally, based on these relationships, the rules for an optimized design for $X_F < X_C$ were obtained.

Keywords: conveyor-belt dryer; food drying; mathematical modeling; design; food quality; food safety

Citation: Friso, D. Mathematical Modelling of Conveyor-Belt Dryers with Tangential Flow for Food Drying up to Final Moisture Content below the Critical Value. *Inventions* **2021**, *6*, 43. https://doi.org/10.3390/inventions6020043

Academic Editor: Chien-Hung Liu

Received: 29 April 2021
Accepted: 10 June 2021
Published: 13 June 2021

1. Introduction

In previous papers [1,2], the conveyor-belt dryer with tangential flow operating in co-current had been indicated as the dryer that shows the advantage of possible lower thermal damage, especially for heat-sensitive food. However, its use is infrequent with respect to the through-circulation conveyor-belt dryer (perforated belt) [1,3]. In fact, having the hot air temperature approximately constant throughout the length of the dryer when the air enters the product, this dryer is more compact and easier to design and, given its high diffusion, it has been the subject of theoretical and experimental studies also to give indications for its design [4–10].

Furthermore, the thermo-hygrometric exchanges during drying are described by differential equations [11] that can be solved in closed form or with numerical methods. The scientific literature is rich in mathematical models of heat and mass exchanges developed with numerical or empirical solutions to describe the drying phenomenon when the temperature of the air entering or touching the product remains constant. Among the food products that can be mentioned are: apple [12–17], apricot [18], banana [19–23], carrot [24], cassava [25], coconut [26], coroba [27], cumbeba [28], fisher [29], ginger [30], jujuba [31], kiwi [32], mandarin [33], mango [34–37], mussel [38], quince [39], papaya [40], pear [41], potato [42], rice [43], sultanas [44], taraxacum [45], tomato [46,47], turnip [48], generic fruits [49–54] and generic foods [55–71].

Trying to fill the gap in the study of conveyor-belt dryers with tangential flow, in a previous work [1] mathematical modelling was developed of the thermo-hygrometric exchanges between the product with final moisture content X_F higher than the critical one

X_C ($X_F > X_C$) and the air that continuously changes its temperature inside the dryer in order to offer a series of design guidelines. In the present work, with the aim of completing the study related to the case of final moisture content of the product lower than the critical one ($X_F < X_C$), broader mathematical modelling will be performed for these dryers. Finally, after the experimental validation of the mathematical modelling, the design guidelines will be proposed.

2. Materials and Methods

2.1. Mathematical Modelling

Figure 1 shows the schematic of a conveyor-belt dryer with tangential flow. The typical diagram of the temperatures of the air T_A and the product T_P inside the dryer is also shown. Inside, two zones can be identified: first long $L_{I\text{-}C}$, where the product maintains the moisture content X higher than the critical moisture content X_C and, last, long $L_{C\text{-}E}$ where the moisture content of the product X is lower than the critical one X_C.

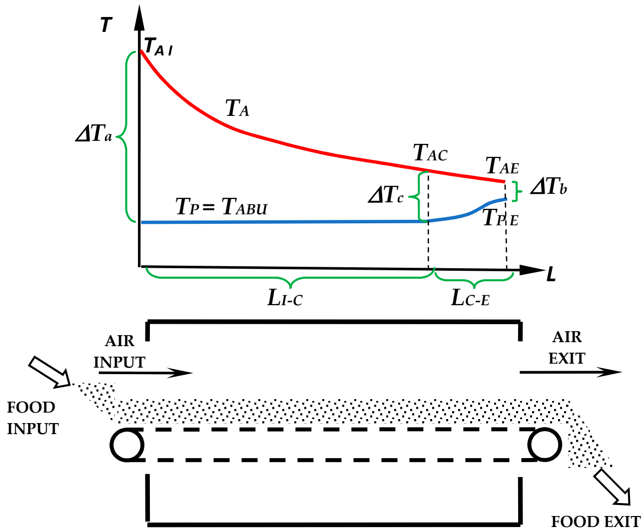

Figure 1. The conveyor-belt dryer with tangential flow and diagram of the temperature of the air and product with final moisture content X_F lower than the critical one X_C ($X_F < X_C$).

2.1.1. First Zone of the Dryer $L_{I\text{-}C}$

In the first zone, long $L_{I\text{-}C}$, the product is characterized by a moisture content X higher than the critical one X_C, and therefore it maintains its temperature T_P constant and equal to the wet bulb temperature T_{WB} [1]. In this first zone, the equations proposed in the previous work [1] are valid. The first equation, called (12) in [1], concerns the heat transfer rate $q_{I\text{-}C}$ that the warm and dry air of initial mass flow rate G_{AI} releases when cooling from the input temperature T_{AI} to temperature T_{AC} corresponding to the achievement of critical moisture content (Figure 1):

$$q_{I-C} = G_{AI} \cdot c_A (T_{AI} - T_{AC}) \cdot \eta \quad (1)$$

where: c_A is the specific heat of dry air; η is the corrective coefficient introduced in [2] and related to the heat losses. For the pilot dryer used in the experiments performed in this work, η is equal to 0.965.

The second equation, called (13) in [1], concerns the heat transfer rate $q_{I\text{-}C}$ exchanged between the air and the product:

$$q_{I-C} = \alpha \cdot A_{I-C} \cdot \Delta T_{mL(I-C)}$$

where: α is the convective heat transfer coefficient; $\Delta T_{mL(I\text{-}C)}$ is the logarithmic mean temperature difference in the I-C zone; $A_{I\text{-}C}$ is the total area of the product inside the I-C zone of the dryer.

From Equation (18) of [1]: $A_{I-C} = f \cdot L_{I-C}$; where: f is the transverse dimension shown in Figure 5 of [1]; $L_{I\text{-}C}$ is the length of the I-C zone of the dryer (Figure 1). Therefore, the equation that gives the heat transfer rate exchanged between air and product is:

$$q_{I-C} = \alpha \cdot f \cdot L_{I-C} \cdot \Delta T_{mL(I-C)} \tag{2}$$

The third equation refers to the heat transfer rate required by the water in the product to evaporate. It was indicated with the number (20) in [1]:

$$q_{I-C} = G_{EV(I-C)} \cdot r_{I-C} = H_I \cdot B_I \cdot v_{Belt} \cdot \rho_{BulkI} \cdot \frac{X_I - X_C}{1 + X_I} \cdot r_{I-C} \tag{3}$$

where: $G_{EV(I\text{-}C)}$ is the mass flow rate of the evaporated water in the I-C zone; H_I is the input height and B_I is the input width of the bulk product on the belt; v_{Belt} is the belt speed; ρ_{BulkI} is the bulk density of the input product; X_I is the input moisture content; X_C is the critical moisture content; $r_{I\text{-}C}$ is the thermal energy, in the I-C zone, required to produce 1 kg of superheated steam at the air temperature T_A; $r_{I\text{-}C}$ is equal to the difference in enthalpy [3] between the superheated steam at T_A and the water contained in the product to be dried at the temperature T_P. As indicated in [1] $r_{I\text{-}C}$ is considered constant and has an average value of 2617 kJ kg^{-1}.

2.1.2. Second Zone of the Dryer $L_{C\text{-}E}$

In order to write the mathematical modelling of the C-E drying zone in which the product moisture content is lower than the critical one ($X < X_C$), the first equation proposed concerns the heat transfer rate $q_{C\text{-}E}$ that the warm air of initial flow rate G_{AI} releases when cooling from the temperature T_{AC} to the exit temperature T_{AE}. This equation is similar to (1):

$$q_{c-E} = G_{AI} \cdot c_A (T_{AC} - T_{AE}) \cdot \eta \tag{4}$$

where: G_{AI} is the mass flow rate of drying air; c_A is its specific heat; η is the corrective coefficient introduced in [2], related to the heat losses and equal to 0.965 for the pilot dryer used in the experiments. The steam mass flow rate coming from the previous $L_{I\text{-}C}$ dryer area and mixed with the air, has been neglected because analyzing the data indicated in [1] it is about 2% of the dry air flow rate G_{AI} and therefore two orders of magnitude less than G_{AI}.

The second equation, concerning the heat transfer rate $q_{C\text{-}E}$ exchanged between air and product, is similar to (2):

$$q_{C-E} = \alpha \cdot f \cdot L_{C-E} \cdot \Delta T_{mL(C-E)} \tag{5}$$

where: α is the convective heat transfer coefficient; $\Delta T_{mL(C\text{-}E)}$ is logarithmic mean temperature difference in the C-E zone; f is the transverse dimension shown in Figure 5 of [1]; $L_{C\text{-}E}$ is the length of the C-E zone of the dryer (Figure 1).

The third equation refers to the heat transfer rate $q_{C\text{-}E}$ required by the water to evaporate and, similarly to (3), it is:

$$q_{C-E} = G_{EV(C-E)} \cdot r_{C-E} = H_I \cdot B_I \cdot v_{Belt} \cdot \rho_{BulkC} \cdot \frac{X_C - X_F}{1 + X_C} \cdot r_{C-E} \tag{6}$$

where: $G_{EV(C\text{-}E)}$ is the mass flow rate of the evaporated water in the C-E zone; H_I is the input height and B_I is the input width of the bulk product on the belt; v_{Belt} is the belt speed; ρ_{BulkC} is the bulk density in the point where the product has the critical moisture content; X_C is the critical moisture content; X_F is the final moisture content; $r_{C\text{-}E}$ is the thermal energy, in the C-E zone, required to produce 1 kg of superheated steam at the air temperature T_A and is equal to the difference in enthalpy [3] between the superheated steam at T_A and the water contained in the product to be dried at the temperature T_P. The thermal energy $r_{C\text{-}E}$ is currently unknown.

A fourth equation must be added to correlate the bulk density ρ_{BulkC} of the product at point C to the input bulk density ρ_{BulkI}.

Considering: $\rho_{BulkI} = \frac{m_D + m_{WI}}{V}$; and: $\rho_{BulkC} = \frac{m_D + m_{WC}}{V}$, where: m_D is the dry mass; m_W is the mass of water; V is the bulk volume; we obtain:

$$\frac{\rho_{BulkC}}{\rho_{BulkI}} = \frac{1 + X_C}{1 + X_I} \tag{7}$$

Finally, the $L_{C\text{-}E}$ zone with $X < X_C$ is characterized by a drying constrained to the process of internal diffusion of water towards the surface of the product. The diffusion of water inside the product is described by Fick's second law, i.e., by a partial differential equation (PDE) that in the one-dimensional case is: $\frac{\partial X}{\partial t} = D\frac{\partial^2 X}{\partial y^2}$.

In the case of a simple geometry such as the thin plate to which many food products are similar and excluding the initial period corresponding to the phenomenon of delay, Perry [72] suggests a solution of the PDE, such as:

$$\frac{X - X_{eq}}{X_C - X_{eq}} = \frac{8}{\pi^2} e^{-\frac{D \cdot \pi^2}{4 \cdot \delta^2} t} \tag{8}$$

where: X is the moisture content as a function of the drying time t; X_C is the critical moisture content of the product and corresponds to the initial one of the drying in the $L_{C\text{-}E}$ zone; X_{eq} is the equilibrium moisture content; D is the mass diffusivity of water inside the product; δ is half the thickness of the plate.

By differentiating we obtain:

$$\frac{dX}{dt} = -\left(X_C - X_{eq}\right) \cdot \frac{2D}{\delta^2} \cdot e^{-\frac{D \cdot \pi^2}{4 \cdot \delta^2} t} \tag{9}$$

Since [1]: $\frac{dX}{dt} = -\frac{G_{EV}}{m_D}$, where: G_{EV} is the instantaneous mass flow rate of evaporated water; m_D is the dry mass present in the $L_{C\text{-}E}$ section of the dryer and is [2]: $m_D = \frac{H_I \cdot B_I \cdot \rho_{BulkC} \cdot L_{C-E}}{1 + X_C}$, that is, based on (7): $m_D = \frac{H_I \cdot B_I \cdot \rho_{BulkI} \cdot L_{C-E}}{1 + X_I}$. Furthermore, since the belt speed v_{Belt} is constant and: $v_{Belt} = \frac{z}{t}$, the previous (9) becomes:

$$G_{EV} = \frac{H_I \cdot B_I \cdot \rho_{BulkI} \cdot L_{C-E}}{1 + X_I} \cdot \frac{2D}{\delta^2} \cdot \left(X_C - X_{eq}\right) \cdot e^{-\frac{D \cdot \pi^2}{4 \cdot \delta^2 \cdot v_{Belt}} z} \tag{10}$$

This equation indicates that the mass flow rate of water evaporated G_{EV} varies along the horizontal coordinate z within the $L_{C\text{-}E}$ zone of the dryer (Figure 1) according to the exponential function as shown in Figure 2.

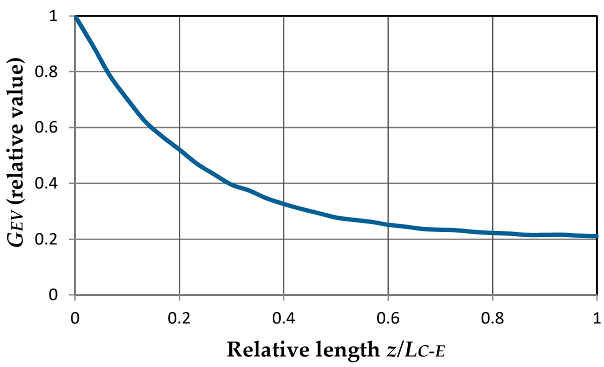

Figure 2. Mass flow rate of evaporated water G_{EV} vs. z-coordinate within the $L_{C\text{-}E}$ zone, corresponding to the direction of the belt in the C-E zone where the moisture content is $X < X_C$.

Therefore, the integral average evaporated water flow rate $G_{EV(C\text{-}E)}$ can be calculated as follows:

$$G_{EV(C-E)} = \frac{1}{L_{C-E}} \int_0^{L_{C-E}} \frac{H_I \cdot B_I \cdot \rho_{BulkI} \cdot L_{C-E}}{1+X_I} \cdot \frac{2D}{\delta^2} \cdot \left(X_C - X_{eq}\right) \cdot e^{-\frac{D \cdot \pi^2}{4 \cdot \delta^2 \cdot v_{Belt}} z} dz$$

Then:

$$G_{EV(C-E)} = \frac{H_I \cdot B_I \cdot \rho_{BulkI} \cdot v_{Belt}}{1+X_I} \cdot \frac{8}{\pi^2} \cdot \left(X_C - X_{eq}\right) \cdot \left[1 - e^{-\frac{D \cdot \pi^2}{4 \cdot \delta^2 \cdot v_{Belt}} L_{C-E}}\right] \tag{11}$$

However, since food products do not always have the plate shape, the previous equation must be rewritten to make the mathematical model more general:

$$G_{EV(C-E)} = \frac{H_I \cdot B_I \cdot \rho_{BulkI} \cdot v_{Belt}}{1+X_I} \cdot C_1 \cdot \left(X_C - X_{eq}\right) \cdot \left[1 - e^{-\frac{C_2}{v_{Belt}} L_{C-E}}\right] \tag{12}$$

where: C_1 and C_2 are constants to be determined by experiments.

The heat flow rate required for this mass flow rate of evaporated water is:

$$q_{C-E} = \frac{H_I \cdot B_I \cdot \rho_{BulkI} \cdot v_{Belt}}{1+X_I} \cdot C_1 \cdot \left(X_C - X_{eq}\right) \cdot \left[1 - e^{-\frac{C_2}{v_{Belt}} L_{C-E}}\right] \cdot r_{C-E} \tag{13}$$

Equation (13) is added to the other four Equations (4)–(7) to perform mathematical modelling of the drying in the $L_{C\text{-}E}$ zone where the moisture content is $X < X_C$.

2.2. Design Guidelines

In the previous paragraph, eight equations were found, namely (1), (2), (3), (4), (5), (6), (7) and (13), in which there are eight unknowns: $q_{I\text{-}C}$, $q_{C\text{-}E}$, G_{AI}, ρ_{BulkI}, T_{AC}, $L_{I\text{-}C}$, $L_{C\text{-}E}$ and T_{PE}. Therefore, this system of equations has a solution, which will be found in the next sub-paragraphs, where the design guidelines will be also proposed.

2.2.1. Air Temperature T_{AC} at Critical Moisture Content of the Product

Since the air temperature at the input T_{AI} and exit T_{AE} of the dryer can be imposed a priori [1], the combination of Equations (1) and (3) gives:

$$G_{AI} \cdot c_A \cdot (T_{AI} - T_{AC}) \cdot \eta = H_I \cdot B_I \cdot v_{Belt} \cdot \rho_{BulkI} \cdot \frac{X_I - X_C}{1+X_I} \cdot r_{I-C} \tag{14}$$

The combination of Equation (4) with (6) and (7) gives:

$$G_{AI} \cdot c_A \cdot (T_{AC} - T_{AE}) \cdot \eta = H_I \cdot B_I \cdot v_{Belt} \cdot \rho_{BulkI} \cdot \frac{X_C - X_F}{1+X_I} \cdot r_{C-E} \tag{15}$$

The division of (14) with (15), after a few steps, gives the T_{AC} temperature (Figure 1):

$$T_{AC} = \frac{T_{AE} \cdot (X_I - X_C) \cdot r_{I-C} + T_{AI} \cdot (X_C - X_F) \cdot r_{C-E}}{(X_I - X_C) \cdot r_{I-C} + (X_C - X_F) \cdot r_{C-E}} \tag{16}$$

The T_{AC} value allows us to calculate ΔT_c (Figure 1): $\Delta T_c = (T_{AC} - T_{WB})$, where T_{WB} is the temperature of the product equal to the wet bulb temperature [1].

2.2.2. Length of Dryer $L_{I\text{-}C}$ to Reach Critical Moisture Content X_C

The combination of Equation (2) with (3) and the observation [1] that $\frac{f \cdot \alpha}{H_I \cdot B_I} = F \cdot \alpha$, where F is the form factor of the product, gives the length of the dryer $L_{I\text{-}C}$ corresponding to the zone with $X > X_C$:

$$L_{I-C} = \frac{v_{Belt} \cdot \rho_{BulkI} \cdot r_{I-C}}{F \cdot \alpha \cdot \Delta T_{mL(I-C)}} \cdot \frac{X_I - X_C}{1 + X_I} \tag{17}$$

Equation (17) is similar to (23) of [1].

2.2.3. Mass Flow Rate of Drying Air G_{AI}

The combination of Equation (1) with (3) gives the mass flow rate of drying air G_{AI}:

$$G_{AI} = \frac{B_I \cdot H_I \cdot v_{Belt} \cdot \rho_{BulkI}}{c_A \cdot (T_{AI} - T_{AC}) \cdot \eta} \cdot \frac{X_I - X_C}{1 + X_I} \cdot r_{I-C} \tag{18}$$

2.2.4. Length of Dryer $L_{C\text{-}E}$ to Reduce Moisture Content from Critical Value X_C to Final One X_F

The combination of Equation (4) with (13), gives the length of the dryer $L_{C\text{-}E}$ where the product dries from X_C to X_F:

$$L_{C-E} = -\frac{v_{Belt}}{C_2} \cdot \ln\left[1 - \frac{G_{AI} \cdot c_A \cdot (T_{AC} - T_{AE}) \cdot \eta}{C_1 \cdot H_I \cdot B_I \cdot \rho_{BulkI} \cdot v_{Belt} \cdot r_{C-E}} \cdot \frac{1 + X_I}{X_C - X_{eq}}\right] \tag{19}$$

2.2.5. Temperature Difference Δt_b at the Dryer Exit and Product Exit Temperature T_{PE}

The combination of Equation (4) with (5) gives the temperature difference between the air and the product at the exit of the dryer (Figure 1): $\Delta T_b = T_{AE} - T_{PE}$, where T_{AE} is the air exit temperature and T_{PE} is the product exit temperature:

$$\Delta T_{mL(C-E)} = \frac{\Delta T_c - \Delta T_b}{\ln \frac{\Delta T_c}{\cdot T_b}} = \frac{G_{AI} \cdot c_A \cdot (T_{AC} - T_{AE}) \cdot \eta}{F \cdot \alpha \cdot H_I \cdot B_I \cdot L_{C-E}}. \tag{20}$$

The temperature difference ΔT_b can be obtained by an iterative method easily through a spreadsheet. As seen in Section 2.2.1, the T_{AE} temperature can be set a priori and, therefore, the product exit temperature $T_{PE} = T_{AE} - \Delta T_b$ can be obtained.

2.2.6. Known Quantities and Experimental Quantities

a. The input and exit temperatures of the drying air T_{AI} and T_{AE} can be defined using the guidelines 3.1.1 proposed in [1].
b. The compound quantity $F \cdot \alpha$ is the product of the convective heat transfer coefficient α and the form factor $F = \frac{f}{H_I \cdot B_I}$, where f is the transverse dimension (Figure 5 in [1]) and H_I and B_I are the height and width of the bulk product placed above the belt, respectively. The quantity $F \cdot \alpha$ is measured as indicated in the guidelines 3.1.9 of [1].
c. The bulk density ρ_{BulkI} is measured as indicated in the next point I) of Section 2.3.
d. The thermal energy $r_{I\text{-}C}$ has an average value of 2617 kJ kg^{-1}, as indicated in guidelines 3.1.6 of [1].

e. The constants C_1 and C_2, where the first one can be connected to the diffusivity of the water inside the product and to the size and the second concerns the initial delay, must be determined using the experimental method that will be described in the next Section 2.3. The same experimental method will also allow us to determine the critical moisture content X_C and the equilibrium moisture content X_{eq}.

f. To determine the lengths $L_{I\text{-}C}$ and $L_{C\text{-}E}$ of the dryer, it is necessary to impose the belt speed v_{Belt} and the height H_I and the width B_I of the bulk product above the belt. These three quantities must be chosen a priori in order to reach the total mass flow rate of evaporated water $G_{EV(I\text{-}E)}$ foreseen for the dryer. In fact, it is known that the quantity characterizing a dryer, both technically and commercially, is the $G_{EV(I\text{-}E)}$ quantity. Therefore, the designer must start from: a known value of the mass flow rate $G_{EV(I\text{-}E)}$; the input and final moisture content and from bulk density of the product; an equation obtained by adding the mass flow rate of evaporated water $G_{EV(I\text{-}C)}$ in the $L_{I\text{-}C}$ zone, and the one $G_{EV(C\text{-}E)}$ of the $L_{C\text{-}E}$ zone:

$$G_{EV(I-E)} = G_{EV(I-C)} + G_{EV(C-E)} = H_I \cdot B_I \cdot v_{Belt} \cdot \rho_{BulkI} \frac{X_I - X_F}{1 + X_I} \tag{21}$$

In this equation, the designer can choose the values of H_I, B_I and hence can obtain the v_{Belt}.

g. Finally, the thermal energy $r_{C\text{-}E}$ in the $L_{C\text{-}E}$ length zone with $X < X_C$ must be measured. The $r_{C\text{-}E}$ will be greater than the $r_{I\text{-}C}$ of the zone with $X > X_C$, since below a certain value of the moisture content X, lower than the critical one X_C, the evaporation of the bound water requires thermal energy greater than that for free-form water. In Section 2.3 the iterative method for determining the experimental values of $r_{C\text{-}E}$ will be described.

2.3. Experimental Procedure and Equipment

The experimental activity was carried out using a pilot dryer. The pilot dryer was the same as in previous works [1,2] and Table 1 summarizes its geometrical data. All the tests were carried out by drying alfalfa consisting of leaves attached to the stems cut in pieces 5 cm long. In the table the value of the quantity $F \cdot \alpha$ relative of alfalfa is also reported. This quantity $F \cdot \alpha$ was experimentally evaluated in the previous work [1].

The measuring instruments used were: infrared thermometer for the alfalfa temperature; PT100 resistance thermometers for the input and exit temperature of the dryer; precision balance for weighing the sample before and after dehydration in an oven for two hours at 135 °C to measure the moisture content of the product at the input and exit; a pitot anemometer; data logger. The bulk density was calculated after measuring the mass and volume of the samples. Five replicates were made for each test.

Table 1. Geometrical and operational data of the pilot dryer.

Quantity	Symbol	Value
Belt width	B_I (m)	0.3
Total Belt length	L_T (m)	6.0
Alfalfa bulk height	H_I (m)	0.05
Flow section of the drying air	A_A (m^2)	0.15
Form factor·Convective heat transfer coefficient [1]	$F \cdot \alpha$ (W·m^{-3}·K^{-1})	5144

The three purposes of the experiments were:

(I) to quantify the constants C_1, C_2, the critical moisture content X_C and the equilibrium moisture content X_{eq} of the alfalfa were as foreseen in the previous point **e.** of Section 2.2.6. The four quantities, C_1, C_2, X_C and X_{eq} can be obtained from the experimental drying curve plotted in a diagram (time, moisture content), by interpolating the moisture content data measured each minute on a sample of the product inserted in the pilot dryer. The sample of alfalfa of initial moisture content X_I was placed with a height H_I equal to 0.05 m on a thin aluminum plate 1 m long and 0.3 m wide, i.e., like the dryer belt width. In turn, the plate was placed on a precision balance placed on the locked belt of the dryer. Only the drying air at the temperature T_{AI} equal to 60 °C was forced by the fan to lick the product sample. The total mass of the sample $m_T = m_W + m_D$, dry mass m_D plus water mass m_W, was measured each minute. Knowing [2] that $m_D = \frac{m_{TI}}{1+X_I}$, where m_{TI} is the initial mass of the sample, the moisture content X of the product at instant t in which the mass of the alfalfa sample m_T is measured, can be calculated as follows:

$$X = \frac{m_T}{m_D} - 1 = \frac{m_T}{m_{TI}}(1 + X_I) - 1 \tag{22}$$

where the initial moisture content X_I is measured on a separate sample of the same alfalfa, by weighing the mass before and after drying in an oven at 135 ° C for two hours. Therefore, the drying curve plotted on the *t*-*X* diagram allows obtaining C_1, C_2, X_C and X_{eq} (see also the next Section 3);

(II) to quantify the thermal energy $r_{C\text{-}E}$ during drying with $X<X_C$ by means of an iterative procedure as provided in point **g.** of the previous Section 2.2.6. The iterative procedure consists of *three steps*. In the *first step*, $r_{C\text{-}E}$ is assumed equal to $r_{I\text{-}C}$ that is 2617 kJ kg^{-1} and a preliminary design of the dryer is performed according to guidelines Section 2.2. However, some guidelines are overturned because the pilot dryer already has a predetermined length $L_T = L_{I\text{-}C} + L_{C\text{-}E} = 6$ m. Therefore, in this case the sequence of calculations is seen to impose $L_T = 6$ m to derive the belt speed v_{Belt}. For the rest of the quantities, the guidelines are the same as in Section 2.2, thus determining the air temperature T_{AC} and T_{AE}, the mass flow rate of the drying air G_{AI} and the product exit temperature T_{PE}, using equations in the Section 2.2.1, Section 2.2.3 and Section 2.2.5. The *second step* consists in carrying out a test on the pilot dryer functioning as required by the preliminary design. During the test, the actual temperatures T'_{PE} and T'_{AE} are measured, which will be different from those of the preliminary design T_{PE} and T_{AE}. The *third step* consists in looking for the $r_{C\text{-}E}$ value which, inserted in the equations of guidelines Section 2.2, allows to restore the initial values of the T_{PE} and T_{AE} temperatures of the preliminary project, to the experimental values T'_{PE} and T'_{AE}. Since the equations of guidelines Section 2.2 are implementable in a spreadsheet, it is very easy to perform this *third step*;

(III) to validate the mathematical model described in Section 2.1 and the design guidelines described in Section 2.2.

3. Results

To determine the quantities X_C, X_{eq}, C_1 and C_2, the series of tests was conducted as described in **purpose (I)** of the previous Section 2.3. Figure 3 shows the time-moisture content diagram (*t*-*X*) called drying curve. The value of the critical moisture content X_C was measured at the point where the straight section, which represents the drying phase at constant rate ($dX/dt = R_C$), begins to flex, exactly when the derivative dX/dt changes by 1% with respect to the value of the slope of the line equal to R_C.

When the measured moisture content value remained constant for five consecutive readings (5 min), it was defined as the equilibrium moisture content X_{eq}.

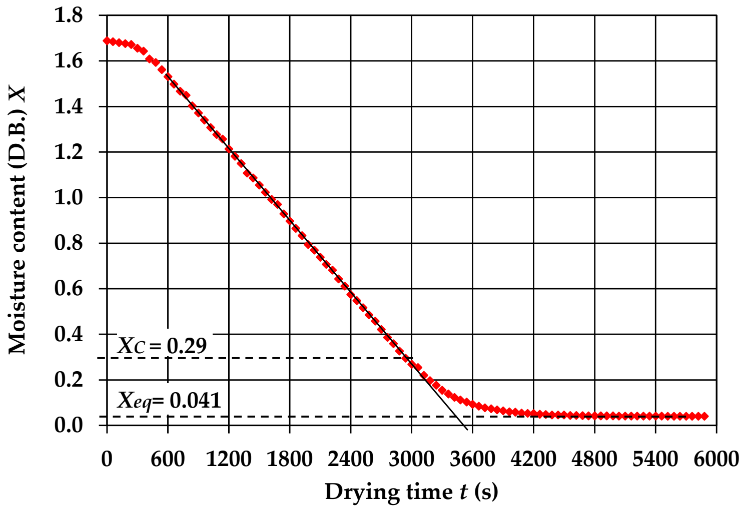

Figure 3. Experimental drying curve of alfalfa. From it, the critical moisture content X_C and the equilibrium moisture content X_{eq} can be obtained.

To determine the constants C_1 and C_2, the diagram of Figure 4 was made using data of Figure 3 relating to the phase with decreasing drying rate, i.e., for $X \leq X_C$. In fact, the time on the abscissa is $t' = t - t_C$, where t_C is the time to reach the critical moisture content X_C. In ordinate there is the quantity: $\ln\left(\frac{X-X_{eq}}{X_C-X_{eq}}\right)$.

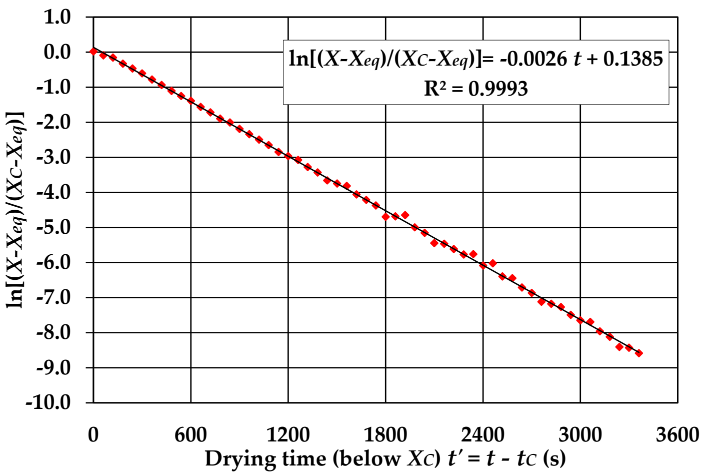

Figure 4. Alfalfa drying curve modified to obtain the constants C_1 and C_2, the first can be linked to the diffusivity of the water inside the product and to the size, the second to the initial delay.

Starting from Equation (13) and returning to having time as an independent variable, it becomes:

$$\ln \frac{X - X_{eq}}{X_C - X_{eq}} = \ln C_1 - C_2 \cdot t \quad (22)$$

This is the equation of a line that has a negative slope equal to $-C_2$ and intercept equal to $\ln(C_1)$, therefore it is sufficient to look for the regression line in the diagram of Figure 4, to obtain $\ln(C_1) = 0.1385$ and $C_2 = 0.0026$. Table 2 summarizes the results obtained.

Table 2. Results from experimental drying curve.

Quantity	Symbol	Value
Alfalfa input moisture content (D.B.)	X_I	1.688 ± 0.105
Alfalfa input bulk density	ρ_{BulkI} (kg·m^{-3})	183 ± 7.6
Alfalfa critical moisture content (D.B.)	X_C	0.290
Alfalfa equilibrium moisture content (D.B.)	X_{eq}	0.041
Coefficient related to delay	C_1	1.149
Coefficient related to diffusivity	C_2	0.0026

To determine the average thermal energy $r_{C\text{-}E}$ required to evaporate 1 kg of water during drying with $X < X_C$, the procedure adopted is that described in purpose II) of the previous Section 2.3. The results of the three steps are indicated in Table 3.

Table 3. Results of the three steps to obtain the thermal energy $r_{C\text{-}E}$ concerning the humidity $X < X_C$. The first step refers to the results of the preliminary design with $r_{C\text{-}E}$ equal to $r_{I\text{-}C}$ = 2617 kJ/kg. The second step concerns the experimental measurement of moisture content and temperatures of the air and of the product (red font). The third step concerns the $r_{C\text{-}E}$ value found (red font) through the equations of the design guidelines 2.3 by imposing the experimental temperatures (red font).

Quantity	Symbol	1st Step Preliminary Design	2nd Step Exper. Value	3rd Step Search for $r_{C\text{-}E}$
Thermal energy	$r_{C\text{-}E}$ (kJ kg^{-1})	2617		4271
Input moisture content	X_I	1.688	1.688 ± 0.105	1.688
Final moisture content	X_F	0.122	0.121 ± 0.01	0.122
Input bulk density	ρ_{BulkI} (kg m^{-3})	183	183 ± 7.6	183
Critical moisture content	X_C	0.290	=	0.290
Equilibrium moisture content	X_{eq}	0.041	=	0.041
Air input temperature	T_{AI} (°C)	120	119.7 ± 1.2	120
Air exit temperature	T_{AE} (°C)	57	52.7 ± 1.1	52.7
Belt velocity	v_{Belt} (m s^{-1})	0.0036	=	0.0036
Air temperature in C	T_{AC} (°C)	63.8	=	63.8
Dryer length I-C (Figure 1)	$L_{I\text{-}C}$ (m)	3.55	=	3.55
Dryer length C-E (Figure 1)	$L_{C\text{-}E}$ (m)	2.45	=	2.45
Total dryer length	L_T (m)	6.00	=	6.00
Product exit temperature	T_{PE} (°C)	55.6	46.5 ± 0.7	46.5
Air input mass flow rate	G_{AI} (kg s^{-1})	0.246	0.246 ± 0.006	0.246

During the first step, the dryer was preliminarily designed by imposing a thermal energy in the C-E section, where $X < X_C$, $r_{C\text{-}E}$ is 2617 kJ/kg, i.e., the same as in the I-C section, where $X > X_C$. In addition, a total length L_T equal to 6 m was set for this preliminary design, which is the length of the pilot dryer (Table 1), in order to obtain the belt speed v_{Belt}, through the design guidelines of Section 2.2. Instead, the belt speed v_{Belt} is normally chosen, so that the mass flow rate of evaporated water $G_{EV(I\text{-}E)}$ foreseen for the dryer is satisfied through Equation (21), and consequently, through the design guidelines 2.2, the length L_T is calculated.

Therefore, the data of the first column (first step) are related to this preliminary design (blue font). In the second step, it was planned to carry out the experimental survey on the pilot dryer, running with the data obtained in the first step. Among the experimental measurements detected, the most important were the product exit temperature T_{PE} (red font) and the air exit temperature T_{AE} (red font). As reported in the second column (*2nd step*) of Table 3, the values of these quantities are lower than those expected from the preliminary design: an experimental T'_{AE} = 52.7 °C instead of design T_{AE} = 57 °C and an experimental T'_{PE} = 46.5 °C instead of design T_{PE} = 55.6 °C. It is clear the experimental T'_{AE} lower than the design T_{AE} indicates that the air has more cooled to transmit a greater heat flow rate towards the product to be dried. This is an indication that the product requires a thermal energy $r_{C\text{-}E}$ greater than that assumed in the preliminary design, which was 2617 kJ kg^{-1}. The decrease in the experimental T'_{PE} compared to the design T_{PE} can also be explained by the need to transmit a greater heat flow rate to the product due to $r_{C\text{-}E}$ greater than 2617 kJ kg^{-1}. In fact, the experimental T'_{PE} settled on a value that produced a logarithmic mean temperature difference $\Delta T'_{mL(C\text{-}E)}$ of Equation (5) equal to 13.9 °C against the 8.5 °C of the $\Delta T_{mL(C\text{-}E)}$ calculated during the design of the first step. Therefore, the increase in $\Delta T_{mL(C\text{-}E)}$ is 63.2% and implies that the heat flow rate $q_{C\text{-}E}$ has to increase by the same amount based on Equation (5), therefore based on Equation (6) also the thermal energy $r_{C\text{-}E}$ has to increase by 63.2% i.e., from 2617 to 4271 kJ kg^{-1}. This last value coincides with that obtained in the third step (Table 3) according to the procedure of purpose (II) of Section 2.3, confirming that the calculations are correct.

The purpose (III) of the experiments, described in Section 2.3, concerned the validation of the mathematical modelling 2.1 and of the design guidelines 2.2, using the value of the thermal energy $r_{C\text{-}E}$ equal to 4271 kJ kg^{-1} as just determined. For a broader validation, the experiments were doubled with the air input temperature T_{AI} set on two values: 120 °C and 100 °C.

Table 4 shows the results obtained. The values of the quantities in the first column are those of the design carried out according to guidelines 2.3 with T_{AI} equal to 120 °C. The values of the second column are those detected during the test with T_{AI} equal to 120 °C and concern: the product moisture content at the input X_I and at the exit X_F; the input bulk density ρ_{BulkI}; the air exit temperature T_{AE}; the air temperature T_{AC} at point C (Figure 1); the product exit temperature T_{PE}. All the other quantities of the first column (design), particularly the length of the dryer L_T, the mass air flow rate G_{AI} and the speed of the belt v_{Belt} resulted in the same value also during the test (second column) due to the adjustments imposed on the pilot dryer.

The third and fourth columns are similar to the first and second respectively, but with air input temperature T_{AI} equal to 100 °C.

Table 4. Results of the validation of the mathematical modeling and design guidelines.

Quantity	Symbol	*Design*	Exper. Value	*Design*	Exper. Value
Air input temperature	T_{AI} (°C)	***120***	119.7 ± 1.2	***100***	100.9 ± 1.1
Thermal energy ($X > X_C$)	$r_{I\text{-}C}$ (kJ kg^{-1})	2617	=	2617	=
Thermal energy ($X < X_C$)	$r_{C\text{-}E}$ (kJ kg^{-1})	4271	=	4271	=
Input moisture content	X_I	1.688	1.688 ± 0.105	1.688	1.688 ± 0.105
Final moisture content	X_F	0.122	0.120 ± 0.01	0.122	0.124 ± 0.009
Input bulk density	ρ_{BulkI} (kg m^{-3})	183	183 ± 7.6	183	183 ± 7.6
Critical moisture content	X_C	0.290	=	0.290	=
Equilibrium moisture content	X_{eq}	0.041	=	0.041	=
Air exit temperature	T_{AE} (°C)	57	56.7 ± 1.0	57	56.8 ± 0.9
Belt velocity	v_{Belt} (m s^{-1})	0.00369	=	0.00344	=
Air temperature in C	T_{AC} (°C)	67.3	66.9 ± 0.9	64.1	64.3 ± 0.8
Dryer length I-C (Figure 1)	$L_{I\text{-}C}$ (m)	3.47	=	3.64	=
Dryer length C-E (Figure 1)	$L_{C\text{-}E}$ (m)	2.53	=	2.36	=
Total dryer length	L_T (m)	6.00	=	6.00	=
Product exit temperature	T_{PE} (°C)	52	52.4 ± 0.6	52.1	52.2 ± 0.7
Air input mass flow rate	G_{AI} (kg s^{-1})	0.270	0.269 ± 0.006	0.368	0.369 ± 0.005
Evaporated water flow rate	G_{EV} (kg s^{-1})	0.00591	=	0.00550	=

For both T_{AI} of 120 °C and 100 °C, there were no significant differences between the experimental values and the expected ones from the design on: the air exit temperatures T_{AE}; the product exit temperatures T_{PE}; the air temperatures T_{AC} in point C of Figure 1. Even the product exit moisture content X_F did not show significant differences between the experimental values and those expected from the design.

As consequence of these positive results validating mathematical modelling 2.1 and design guidelines 2.2, a part of the equations of the model can be used to extend a result that was obtained in the previous work [2]. In [2], an equation was obtained, numbered (12), which correlated the final moisture content X_F to the air exit temperature T_{AE}, valid for final moisture content greater than the critical one ($X_F > X_C$). In this way, it was possible to indicate the indirect measurement of the final moisture content X_F, useful for optimized adjustment of the drying operation, through the simpler, faster and cheaper measurement of the air exit temperature T_{AE}. Therefore, with the validated equations of the mathematical modelling of Section 2.1 proposed for drying with final moisture content lower than the critical one ($X_F < X_C$), the comparison between (1), (3), (4), (6) and (7) gives the following equation in place of (12) of [2]:

$$X_F = X_C + (X_I - X_C)\frac{r_{I-C}}{r_{C-E}} + \frac{G_{AI} \cdot c_A \cdot (1 + X_I)}{B_I \cdot H_I \cdot v_{Belt} \cdot \rho_{BulkI} \cdot r_{I-C}} \cdot (T_{AE} - T_{AI}) \cdot \eta \tag{24}$$

Knowing the critical moisture content of the product X_C, its input moisture content X_I, its bulk density ρ_{BulkI}, its bulk dimensions on the belt B_I and H_I, the thermal energy values $r_{I\text{-}C}$ and $r_{C\text{-}E}$, the mass flow rate of air G_{AI}, its input temperature T_{AI}, the belt speed v_{Belt} and by measuring the air exit temperature T_{AE}, Equation (24) shows that the final moisture content X_F is promptly obtained. The same equation, appropriately implemented in a PLC, suggests how to correct the X_F, if this is not the expected value, for example by changing the belt speed v_{Belt}, or the air input temperature T_{AI}.

The last result concerns a simulation using the equations of the design guidelines. The influence of the air temperature at the input T_{AI} on the following three variables was analyzed: the length of the dryer L_T; the product temperature at the exit T_{PE}; the mass flow rate of drying air G_{AI}. Since this air temperature at the input T_{AI} is chosen by the designer within a range that depends on the nature of the product [1], the simulation has highlighted the influence of this choice on the three variables defined above. The series of diagrams on the left of Figure 5a–c represents the trend of the three variables as a function of T_{AI} which has values between 100 °C and 150 °C. During the simulation, the following quantities were kept constant: the belt speed v_{Belt} equal to 0.004 m s^{-1}; the air temperature at the exit T_{AE} equal to 60 °C; the mass flow rate of evaporated water in the dryer G_{EV} equal to 23 kg h^{-1}. It is noted that the dryer length decreases significantly. This positive effect is reflected in a more compact system, but there is a slight increase in the product temperature at the exit T_{PE}, by just a couple of degrees, which is therefore acceptable, and a reduction in the mass flow rate of drying air G_{AI} to keep the mass flow rate of evaporated water G_{EV} constant given the increase by T_{AI}. Therefore, the space problem that afflicts these dryers can be mitigated with an increase in T_{AI}.

The series of diagrams on the right of Figure 5d–f provides the three variables—length L_T, temperature T_{PE}, mass flow rate G_{AI}—vs. the air temperature at the exit T_{AE} which is reduced from 60 °C to 50 °C, keeping constant: the belt speed v_{Belt} equal to 0.004 m s^{-1}; the air temperature at the input T_{AI} equal to 120 °C; the mass flow rate of evaporated water in the dryer G_{EV} equal to 23 kg h^{-1}. The figure shows a slight increase in the length of dryer L_T of about 0.5 m (+8%), an important decrease of the product temperature at the exit T_{PE} which decreases from 55.7 °C to 42.8 °C improving the organoleptic and nutritional quality. It should be remembered that the product temperature T_P remains at the wet bulb temperature T_{WB} up to point C (Figure 1) which is located at about 4 m from the input of the dryer. Only in the last 2.75 m, where the moisture content of the product is below the critical one, does the temperature slowly rise up to T_{PE}.

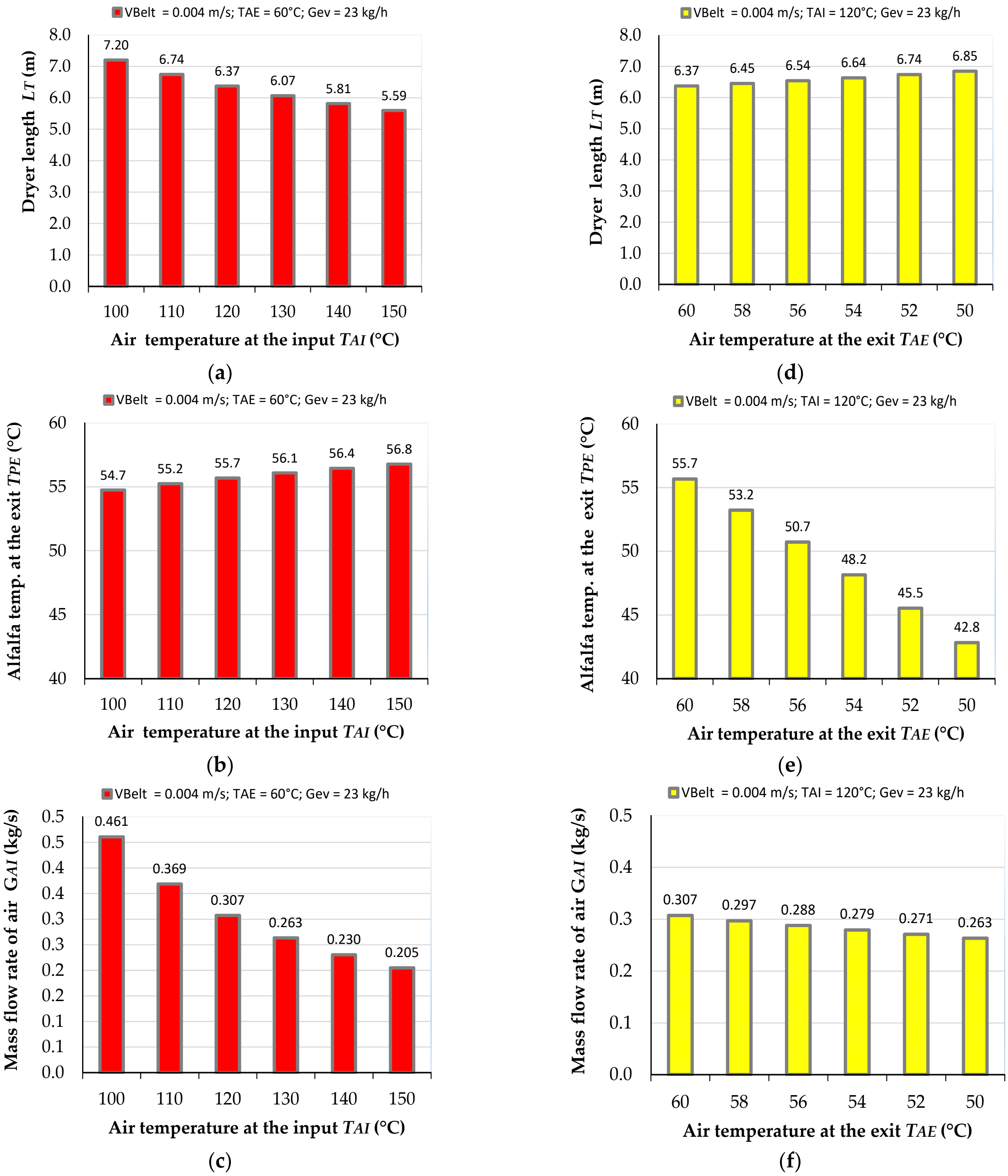

Figure 5. Simulation using the equations of the design guidelines. Left, histograms vs. air temperature at the dryer input T_{AI} (with v_{Belt}, T_{AE} and G_{EV} kept constant), of the: (**a**) dryer length L_T; (**b**) alfalfa temperature at the exit of the dryer T_{PE}; (**c**) mass flow rate of the drying air G_{AI}. Right, histograms of the same variables, but vs. air temperature at the dryer exit T_{AE} with v_{Belt}, T_{AI} and G_{EV} kept constant: (**d**) dryer length L_T; (**e**) alfalfa temperature at the exit of the dryer T_{PE}; (**f**) mass flow rate of the air G_{AI}.

4. Conclusions

In the food industry, the drying operation is still very widespread with the use of various types of system. In this work, the focus was on the conveyor-belt dryer with tangential flow that is underused because it is more cumbersome and more difficult to design, but it has the advantage of greater respect for heat-sensitive food products and, therefore, greater diffusion in the future it may be able to improve food quality. This is the dryer already studied in two previous works [1,2] for the case of final moisture content higher than critical moisture content ($X_F > X_C$). In this work, the mathematical modelling and design guidelines have been extended to the more general situation of a final moisture content lower than the critical one ($X_F < X_C$).

First, all the equations of the thermo-hygrometric exchange have been set up. The associated mathematical modelling allowed us to define design guidelines and also a method to calculate the thermal energy $r_{C\text{-}E}$, necessary to evaporate the water when the moisture content is lower than the critical one ($X < X_C$). In fact, it is always greater than that for $X > X_C$ since starting from a certain moisture content below the critical one X_C, there is bound water which requires higher energy to evaporate compared to latent heat.

Among the eight equations of the mathematical modelling there is one describing the diffusion phenomenon of water inside the product when the moisture content of the product X is lower than the critical one X_C. The mathematical modelling and the equations for the design guidelines, including the method for calculating the thermal energy $r_{C\text{-}E}$, have been experimentally confirmed.

A part of the equations of the mathematical modelling presented here in Section 2.1 was also used to extend the result obtained in a previous work [2] dedicated to drying with the final moisture content of the product exceeding the critical one, $X_F > X_C$. It was an equation that correlated the air exit temperature T_{AE} with the final moisture content of the product X_F which needs to be known promptly and continuously during the operation of the dryer for the optimization and reduction of energy consumption [73] and for the control of thermal damage to the dried product.

Therefore, among the results of this work there is also the new equation extended to the case $X_F < X_C$, able to link the final moisture content X_F to the air exit temperature T_{AE}. If the equation is implemented in a dryer adjustment PLC, it will be able to keep the X_F value constant and optimized, controlling the T_{AE} which is much easier, faster and less expensive to detect than direct methods for measuring the X_F.

Finally, the mathematical modelling and equations of the design guidelines were used to simulate the influence of air temperatures at the input T_{AI} and, respectively, at the exit T_{AE}. This last analysis showed that by reducing the mass flow rate of drying air G_{AI}, with the same T_{AI}, the temperature T_{AE} and consequently the exit temperature of the product T_{PE} can be reduced with, consequently, less thermal damage to food.

Funding: This research received no external funding.

Institutional Review Board Statement: Not applicable.

Informed Consent Statement: Not applicable.

Data Availability Statement: The data presented in this study is contained within the article.

Conflicts of Interest: The author declares no conflict of interest.

References

1. Friso, D. Conveyor-belt dryers with tangential flow for food drying: Mathematical modeling and design guidelines for final moisture content higher than the critical value. *Inventions* **2020**, *5*, 22. [CrossRef]
2. Friso, D. Conveyor-Belt Dryers with Tangential Flow for Food Drying: Development of Drying ODEs Useful to Design and Process Adjustment. *Inventions* **2021**, *6*, 6. [CrossRef]
3. Geankopolis, C.J. *Transport Process Unit Operations*, 3rd ed.; Prentice-Hall International: Englewood Cliffs, NJ, USA, 1993; pp. 520–562.
4. Salemović, D.R.; Dedić, A.D.; Ćuprić, N.L. Two-dimensional mathematical model for simulation of the drying process of thick layers of natural materials in a conveyor-belt dryer. *Therm. Sci.* **2017**, *21*, 1369–1378. [CrossRef]
5. Salemović, D.R.; Dedić, A.D.; Ćuprić, N.L. A mathematical model and simulation of the drying process of thin layers of potatoes in a conveyor-belt dryer. *Therm. Sci.* **2015**, *19*, 1107–1118. [CrossRef]
6. Xanthopoulos, G.; Okoinomou, N.; Lambrinos, G. Applicability of a single-layer drying model to predict the drying rate of whole figs. *J. Food Eng.* **2017**, *81*, 553–559. [CrossRef]

7. Khankari, K.K.; Patankar, S.V. Performance analysis of a double-deck conveyor dryer—A computational approach. *Dry. Technol.* **1999**, *17*, 2055–2067. [CrossRef]
8. Kiranoudis, C.T.; Maroulis, Z.B.; Marinos-Kouris, D. Dynamic Simulation and Control of Conveyor-Belt Dryers. *Dry. Technol.* **1994**, *12*, 1575–1603. [CrossRef]
9. Pereira de Farias, R.; Deivton, C.S.; de Holanda, P.R.H.; de Lima, A.G.B. Drying of Grains in Conveyor Dryer and Cross Flow: A Numerical Solution Using Finite-Volume Method. *Rev. Bras. Prod. Agroind.* **2004**, *6*, 1–16. [CrossRef]
10. Kiranoudis, C.T.; Markatos, N.C. Pareto design of conveyor-belt dryers. *J. Food Eng.* **2000**, *46*, 145–155. [CrossRef]
11. Friso, D. A Mathematical Solution for Food Thermal Process Design. *Appl. Math. Sci.* **2015**, *9*, 255–270. [CrossRef]
12. Askari, G.R.; Emam-Djomeh, Z.; Mousavi, S.M. Heat and mass transfer in apple cubes in a microwave-assisted fluidized bed drier. *Food Bioprod. Process.* **2013**, *91*, 207–215. [CrossRef]
13. Ben Mabrouk, S.; Benali, E.; Oueslati, H. Experimental study and numerical modelling of drying characteristics of apple slices. *Food Bioprod. Process.* **2012**, *90*, 719–728. [CrossRef]
14. Esfahani, J.A.; Vahidhosseini, S.M.; Barati, E. Three-dimensional analytical solution for transport problem during convection drying using Green's function method (GFM). *Appl. Therm. Eng.* **2015**, *85*, 264–277. [CrossRef]
15. Esfahani, J.A.; Majdi, H.; Barati, E. Analytical two-dimensional analysis of the transport phenomena occurring during convective drying: Apple slices. *J. Food Eng.* **2014**, *123*, 87–93. [CrossRef]
16. Golestani, R.; Raisi, A.; Aroujalian, A. Mathematical modeling on air drying of apples considering shrinkage and variable diffusion coefficient. *Dry. Technol.* **2013**, *31*, 40–51. [CrossRef]
17. Jokiel, M.; Bantle, M.; Kopp, C.; Halvorsen Verpe, E. Modelica-based modelling of heat pump-assisted apple drying for varied drying temperatures and bypass ratios. *Therm. Sci. Eng. Prog.* **2020**, *19*, 100575. [CrossRef]
18. Bon, J.; Rossellò, C.; Femenia, A.; Eim, V.; Simal, S. Mathematical modeling of drying kinetics for Apricots: Influence of the external resistance to mass transfer. *Dry. Technol.* **2007**, *25*, 1829–1835. [CrossRef]
19. Baini, R.; Langrish, T.A.G. Choosing an appropriate drying model for intermittent and continuous drying of bananas. *J. Food Eng.* **2007**, *79*, 330–343. [CrossRef]
20. Da Silva, W.P.; Silva, C.M.D.P.S.; Gomes, J.P. Drying description of cylindrical pieces of bananas in different temperatures using diffusion models. *J. Food Eng.* **2013**, *117*, 417–424. [CrossRef]
21. Da Silva, W.P.; Hamawand, I.; Silva, C.M.D.P.S. A liquid diffusion model to describe drying of whole bananas using boundary-fitted coordinates. *J. Food Eng.* **2014**, *137*, 32–38. [CrossRef]
22. Macedo, L.L.; Vimercati, W.C.; da Silva Araújo, C.; Saraiva, S.H.; Teixeira, L.J.Q. Effect of drying air temperature on drying kinetics and physicochemical characteristics of dried banana. *J. Food Process Eng.* **2020**, *43*, e13451. [CrossRef]
23. Kumar, P.S.; Nambi, E.; Shiva, K.N.; Vaganan, M.M.; Ravi, I.; Jeyabaskaran, K.J.; Uma, S. Thin layer drying kinetics of Banana var. Monthan (ABB): Influence of convective drying on nutritional quality, microstructure, thermal properties, color, and sensory characteristics. *J. Food Process Eng.* **2019**, *42*, e13020. [CrossRef]
24. Mahapatra, A.; Tripathy, P.P. Modeling and simulation of moisture transfer during solar drying of carrot slices. *J. Food Process Eng.* **2018**, *41*, e12909. [CrossRef]
25. Thayze, R.B.P.; Pierre, C.M.; Vansostenes, A.M.D.M.; Jacqueline, F.D.B.D.; Daniel, C.D.M.C.; Vital, A.B.D.O.; Iran, R.D.O.; Antonio, G.B.D.L. On the study of osmotic dehydration and convective drying of cassava cubes. *Defect Diffus. Forum* **2021**, *407*, 87–95. [CrossRef]
26. Ramsaroop, R.; Persad, P. Determination of the heat transfer coefficient and thermal conductivity for coconut kernels using an inverse method with a developed hemispherical shell model. *J. Food Eng.* **2012**, *110*, 141–157. [CrossRef]
27. Corzo, O.; Bracho, N.; Pereira, A.; Vàsquez, A. Application of correlation between Biot and Dincer numbers for determining moisture transfer parameters during the air drying of coroba slices. *J. Food Process. Preserv.* **2009**, *33*, 340–355. [CrossRef]
28. Ferreira, J.P.L.; Queiroz, A.J.M.; de Figueirêdo, R.M.F.; da Silva, W.P.; Gomes, J.P.; Santos, D.D.C.; Silva, H.A.; Rocha, A.P.T.; de Paiva, A.C.C.; Chaves, A.D.C.G.; et al. Utilization of cumbeba (Tacinga inamoena) residue: Drying kinetics and effect of process conditions on antioxidant bioactive compounds. *Foods* **2021**, *10*, 788. [CrossRef] [PubMed]
29. Khan, M.A.; Moradipour, M.; Obeidullah, M.; Quader, A.K.M.A. Heat and mass transport analysis of the drying of freshwater fishes by a forced convective air-dryer. *J. Food Process Eng.* **2021**, *44*, e13574. [CrossRef]
30. Osae, R.; Essilfie, G.; Alolga, R.N.; Bonah, E.; Ma, H.; Zhou, C. Drying of ginger slices. Evaluation of quality attributes, energy consumption, and kinetics study. *J. Food Process Eng.* **2020**, *43*, e13348. [CrossRef]
31. Elmas, F.; Varhan, E.; Koç, M. Drying characteristics of jujube (Zizyphus jujuba) slices in a hot air dryer and physicochemical properties of jujube powder. *J. Food Meas. Charact.* **2019**, *13*, 70–86. [CrossRef]
32. Kaya, A.; Aydin, O.; Dincer, I. Experimental and numerical investigation of heat and mass transfer during drying of Hayward kiwi fruits (Actinidia Deliciosa Planch). *J. Food Eng.* **2008**, *88*, 323–330. [CrossRef]
33. Akdas, S.; Baslar, M. Dehydration and degradation kinetics of bioactive compounds for mandarin slices under vacuum and oven drying conditions. *J. Food Process. Preserv.* **2015**, *39*, 1098–1107. [CrossRef]
34. Barati, E.; Esfahani, J.A. A new solution approach for simultaneous heat and mass transfer during convective drying of mango. *J. Food Eng.* **2011**, *102*, 302–309. [CrossRef]
35. Corzo, O.; Bracho, N.; Alvarez, C.; Rivas, V.; Rojas, Y. Determining the moisture transfer parameters during the air-drying of mango slices using biot-dincer numbers correlation. *J. Food Process. Eng.* **2008**, *31*, 853–873. [CrossRef]

36. Janjai, S.; Lamlert, N.; Intawee, P.; Mahayothee, B.; Haewsungcharern, M.; Bala, B.K.; Müller, J. Finite element simulation of drying of mango. *Biosyst. Eng.* **2008**, *99*, 523–531. [CrossRef]
37. Villa-Corrales, L.; Flores-Prieto, J.J.; Xamàn-Villasenor, J.P.; García-Hernàndez, E. Numerical and experimental analysis of heat and moisture transfer during drying of Ataulfo mango. *J. Food Eng.* **2010**, *98*, 198–206. [CrossRef]
38. Kouhila, M.; Moussaoui, H.; Lamsyehe, H.; Tagnamas, Z.; Bahammou, Y.; Idlimam, A.; Lamharrar, A. Drying characteristics and kinetics solar drying of Mediterranean mussel (mytilus galloprovincilis) type under forced convection. *Renew. Energ.* **2020**, *147*, 833–844. [CrossRef]
39. Taghinezhad, E.; Kaveh, M.; Jahanbakhshi, A.; Golpour, I. Use of artificial intelligence for the estimation of effective moisture diffusivity, specific energy consumption, color and shrinkage in quince drying. *J. Food Process Eng.* **2020**, *43*, e13358. [CrossRef]
40. Lemus-Mondaca, R.A.; Zambra, C.E.; Vega-Gàlvez, A.; Moraga, N.O. Coupled 3D heat and mass transfer model for numerical analysis of drying process in papaya slices. *J. Food Eng.* **2013**, *116*, 109–117. [CrossRef]
41. Guiné, R.P. Pear drying: Experimental validation of a mathematical prediction model. *Food Bioprod. Process.* **2008**, *86*, 248–253. [CrossRef]
42. Singh, P.; Talukdar, P. Design and performance evaluation of convective drier and prediction of drying characteristics of potato under varying conditions. *Int. J. Therm. Sci.* **2019**, *142*, 176–187. [CrossRef]
43. Pereira, J.C.A.; da Silva, W.P.; Gomes, J.P.; Queiroz, A.J.M.; de Figueiredo, R.M.F.; de Melo, B.A.; Santiago, A.M.; de Lima, A.G.B.; de Macedo, A.D.B. Continuous and intermittent drying of rough rice: Effects on process effective time and effective mass diffusivity. *Agriculture* **2020**, *10*, 282. [CrossRef]
44. Sabarez, H.T. Mathematical modeling of the coupled transport phenomena and color development: Finish drying of trellis-dried sultanas. *Dry. Technol.* **2014**, *32*, 578–589. [CrossRef]
45. Moussaoui, H.; Idlimam, A.; Lamharrar, A. The characterization and modeling kinetics for drying of taraxacum officinale leaves in a thin layer with a convective solar dryer. *Lect. Notes Electr. Eng.* **2019**, *519*, 656–663. [CrossRef]
46. Obajemihi, O.I.; Olaoye, J.O.; Cheng, J.-H.; Ojediran, J.O.; Sun, D.-W. Optimization of process conditions for moisture ratio and effective moisture diffusivity of tomato during convective hot-air drying using response surface methodology. *J. Food Process Preserv.* **2021**, *45*, e15287. [CrossRef]
47. Obajemihi, O.I.; Olaoye, J.O.; Ojediran, J.O.; Cheng, J.-H.; Sun, D.W. Model development and optimization of process conditions for color properties of tomato in a hot-air convective dryer using box–behnken design. *J. Food Process Preserv.* **2020**, *44*, e14771. [CrossRef]
48. Taghinezhad, E.; Kaveh, M.; Szumny, A. Optimization and prediction of the drying and quality of turnip slices by convective-infrared dryer under various pretreatments by rsm and anfis methods. *Foods* **2021**, *10*, 284. [CrossRef]
49. Castro, A.M.; Mayorga, E.Y.; Moreno, F.L. Mathematical modelling of convective drying of fruits: A review. *J. Food Eng.* **2018**, *223*, 152–167. [CrossRef]
50. Chandra Mohan, V.P.; Talukdar, P. Three dimensional numerical modeling of simultaneous heat and moisture transfer in a moist object subjected to convective drying. *Int. J. Heat Mass Tran.* **2010**, *53*, 4638–4650. [CrossRef]
51. Defraeye, T. When to stop drying fruit: Insights from hygrothermal modelling. *Appl. Therm. Eng.* **2017**, *110*, 1128–1136. [CrossRef]
52. Defraeye, T.; Radu, A. International Journal of Heat and Mass Transfer Convective drying of fruit: A deeper look at the air-material interface by conjugate modeling. *Int. J. Heat Mass Tran.* **2017**, *108*, 1610–1622. [CrossRef]
53. Fanta, S.W.; Abera, M.K.; Ho, Q.T.; Verboven, P.; Carmeliet, J.; Nicolai, B.M. Microscale modeling of water transport in fruit tissue. *J. Food Eng.* **2013**, *118*, 229–237. [CrossRef]
54. Da Silva, W.P.; e Silva, C.M.; e Silva, D.D.; de Araújo Neves, G.; de Lima, A.G. Mass and heat transfer study in solids of revolution via numerical simulations using finite volume method and generalized coordinates for the Cauchy boundary condition. *Int. J. Heat Mass Tran.* **2010**, *53*, 1183–1194. [CrossRef]
55. Aversa, M.; Curcio, S.; Calabro, V.; Iorio, G. An analysis of the transport phenomena occurring during food drying process. *J. Food Eng.* **2007**, *78*, 922–932. [CrossRef]
56. Da Silva, W.P.; Precker, J.W.; e Silva, D.D.; e Silva, C.D.; de Lima, A.G. Numerical simulation of diffusive processes in solids of revolution via the finite volume method and generalized coordinates. *Int. J. Heat Mass Tran.* **2009**, *52*, 4976–4985. [CrossRef]
57. Datta, A.K. Porous media approaches to studying simultaneous heat and mass transfer in food processes. I: Problem formulations. *J. Food Eng.* **2007**, *80*, 80–95. [CrossRef]
58. Defraeye, T. Advanced computational modelling for drying processes—A review. *Appl. Energy* **2014**, *131*, 323–344. [CrossRef]
59. Defraeye, T.; Verboven, P.; Nicolai, B. CFD modelling of flow and scalar exchange of spherical food products: Turbulence and boundary-layer modelling. *J. Food Eng.* **2013**, *114*, 495–504. [CrossRef]
60. Erbay, Z.; Icier, F. A review of thin layer drying of foods: Theory, modeling, and experimental results. *Crit. Rev. Food Sci. Nutr.* **2010**, *50*, 441–464. [CrossRef]
61. Giner, S.A. Influence of Internal and External Resistances to Mass Transfer on the constant drying rate period in high-moisture foods. *Biosyst. Eng.* **2009**, *102*, 90–94. [CrossRef]
62. Khan, F.A.; Straatman, A.G. A conjugate fluid-porous approach to convective heat and mass transfer with application to produce drying. *J. Food Eng.* **2016**, *179*, 55–67. [CrossRef]
63. Lamnatou, C.; Papanicolaou, E.; Belessiotis, V.; Kyriakis, N. Conjugate heat and mass transfer from a drying rectangular cylinder in confined air flow. *Numer. Heat Tran.* **2009**, *56*, 379–405. [CrossRef]

64. Oztop, H.F.; Akpinar, E.K. Numerical and experimental analysis of moisture transfer for convective drying of some products. *Int. Commun. Heat Mass Tran.* **2008**, *35*, 169–177. [CrossRef]
65. Ruiz-Lòpez, I.I.; García-Alvarado, M.A. Analytical solution for food-drying kinetics considering shrinkage and variable diffusivity. *J. Food Eng.* **2007**, *79*, 208–216. [CrossRef]
66. Vahidhosseini, S.M.; Barati, E.; Esfahani, J.A. Green's function method (GFM) and mathematical solution for coupled equations of transport problem during convective drying. *J. Food Eng.* **2016**, *187*, 24–36. [CrossRef]
67. Van Boekel, M.A.J.S. Kinetic modeling of food quality: A critical review. *Compr. Rev. Food Sci. Food Saf.* **2008**, *7*, 144–158. [CrossRef]
68. Wang, W.; Chen, G.; Mujumdar, A.S. Physical interpretation of solids drying: An overview on mathematical modeling research. *Dry. Technol.* **2007**, *25*, 659–668. [CrossRef]
69. Chandramohan, V.P. Convective drying of food materials: An overview with fundamental aspect, recent developments, and summary. *Heat Transf. Asian Res.* **2020**, article in press. [CrossRef]
70. Demirpolat, A.B. Investigation of mass transfer with different models in a solar energy food-drying system. *Energies* **2019**, *12*, 3447. [CrossRef]
71. Çerçi, K.N.; Daş, M. Modeling of heat transfer coefficient in solar greenhouse type drying systems. *Sustainability* **2019**, *11*, 5127. [CrossRef]
72. Perry, R.H. *Chemical Engineers Handbook*, 5th ed.; McGraw-Hill International: Singapore, 1984; pp. 11–20.
73. Friso, D. Energy saving with total energy system for cold storage in Italy: Mathematical modeling and simulation, exergetic and economic analysis. *Appl. Math. Sci.* **2014**, *8*, 6529–6546. [CrossRef]